# PET Imaging of Non-Small-Cell Lung Carcinoma with Carbon-11-Methionine: Relationship Between Radioactivity Uptake and Flow-Cytometric Parameters

Hideki Miyazawa, Takashi Arai, Masaaki Iio and Toshihiko Hara

*Departments of Surgery and Radiology, National Nakano Chest Hospital, Tokyo, Japan*

Carbon-11-methionine PET scans were obtained from 24 patients with non-small-cell lung carcinoma for whom surgical treatment was considered. The tumor mass was visualized with clear delineation. After PET scanning, the tumor was removed by lobectomy or pulmonectomy. The tumor tissue was first processed to yield tumor cell suspensions and then subjected to DNA flow cytometry. Comparison between ^{11}C uptake rate and flow-cytometric data gave the following results: [11]C uptake rate in the tumor correlated well with the cellular DNA content (DNA index) of tumor cells at the resting state of cell division (G0 + G1-phase) (r = 0.67). The correlation between ^{11}C uptake rate and S-phase cell percentage was markedly high (r = 0.76), and the correlation between ^{11}C uptake rate and S + G2/M-phase cell percentage was extremely high (r = 0.86). It was concluded that the tumor uptake rate of ^{11}C-methionine was representive of tumor growth rate in this tumor type.

**J Nucl Med 1993; 34:1886–1891**

$T$he clinical staging of non-small-cell lung carcinoma (NSCLC) depends on the TNM classification. Only the anatomical (morphological) characteristics of the tumors are considered, but the biologic parameters of tumor tissue are not included in this staging procedure. Ploidy and proliferating activity of tumor cells analyzed by flow cytometry are widely accepted as good indicators of tumor malignancy (1–9). The positron-emitting radiopharmaceuticals, L-[methyl-^{11}C]methionine, ^{11}C-methionine and ^{18}F-2-fluoro-2-deoxy-D-glucose ([18]FDG) are widely used for tumor imaging, and the uptake rate of these tracers in tumors have been studied in comparison with flow-cytometric parameters: with [18]FDG in head and neck cancer (10–12), ^{11}C-methionine in breast cancer (13) and ^{11}C-methionine

and [18]FDG in nonHodgkin's lymphoma (14). The purpose of this research was to examine the relationship between ^{11}C-methionine uptake and the flow-cytometric parameters in NSCLC.

Methionine is either utilized for protein synthesis or serves as the biological methyl donor for the methylation of DNA, transfer-RNA and other compounds (transmethylation) after formation of S-adenosylmethionine (SAM). The relative magnitude of these alternates is not well understood. In vitro experiments have shown that cultured cell lines of human tumor (15,16) and activated lymphocytes (lymphoblasts) (17), are extremely dependent on methionine supply in the culture medium because of the reduced activity of methionine synthesis from homocysteine, contrary to all other normal cells. Bustany et al. (18) reported that ^{11}C-methionine accumulation in brain tumors was related to its grade. Leskinen-Kallio et al. (13) reported that the uptake of ^{11}C-methionine in breast cancer was associated with a large S-phase fraction measured with flow cytometry.

Leskinen-Kallio et al. (14) found the correlation of ^{11}C-methionine uptake to S-phase fraction was higher than that of [18]FDG uptake to the S-phase fraction in nonHodgkin's lymphoma. Fujiwara et al. (19) reported that the ^{11}C-methionine uptake in human lung cancers varied among its different histological types. From the above reports it was expected that ^{11}C-methionine could be used for visualizing lung cancer, with the intensity of uptake rate proportional to the tumor growth rate.

The abnormal DNA content (aneuploidy) and proliferative characteristics as shown by S-phase and G2/M-phase cell population can be determined from the tumor cell suspension. It is usually prepared from freshly frozen tissue specimens. The paraffin-embedded material can be employed also, but it is only good for the ploidy analysis (20,21). It has been advised that the cell-phase analysis with the latter material be avoided. In this work, flow cytometry was performed using paraffin blocks and freshly frozen specimens for ploidy analysis. Only freshly frozen

**TABLE 1**
Patient Characteristics

| Patient no.[*] | Age | Sex | Diagnosis[†] | pTNM[‡] | p-stage[§] |
|---|---|---|---|---|---|
| 1 | 56 | F | Adeno | T1N2M0 | IIIA |
| 2 | 77 | M | Squamous | T1N0M0 | I |
| 3 | 59 | M | Squamous | T3N0M0 | IIIA |
| 4 | 69 | F | Adeno | T2N2M0 | IIIA |
| 5 | 66 | F | Adeno | T1N0M0 | I |
| 6 | 61 | M | Squamous | T3N2M1 | IV |
| 7 | 82 | M | Squamous | T4N2M0 | IIIB |
| 8 | 74 | M | Squamous | T2N1M0 | II |
| 9 | 75 | M | Squamous | T1N0M0 | I |
| 10 | 47 | M | Adenosquamous | T4N2M0 | IIIB |
| 11 | 60 | M | Adeno | T3N0M0 | IIIA |
| 12 | 50 | M | Adenosquamous | T3N1M0 | IIIA |
| 13 | 60 | M | Adeno | T1N0M0 | I |
| 14 | 57 | M | Squamous | T1N0M0 | I |
| 15 | 46 | M | Adeno | T2N1M0 | II |
| 16 | 67 | M | Squamous | T2N2M0 | IIIA |
| 17 | 55 | M | Squamous | T3N1M0 | IIIA |
| 18 | 67 | M | Adeno | T2N2M0 | IIIA |
| 19 | 73 | M | Squamous | T2N2M0 | IIIA |
| 20 | 71 | M | Adeno | T2N0M0 | I |
| 21 | 55 | M | Squamous | T3N0M0 | IIIA |
| 22 | 60 | M | Adeno | T3N0M0 | IIIA |
| 23 | 60 | M | Squamous | T3N0M0 | IIIA |
| 24 | 46 | M | Adeno | T2N1M0 | II |

[*]Corresponds to Table 2.
[†]Histological diagnosis determined on surgically resected material: Adeno = adenocarcinoma; Squamous = squamous-cell carcinoma; and Adenosquamous = adenosquamous carcinoma.
[‡]Pathological TNM classification.
[§]Pathological stage.

specimens were used for the S-phase and G2/M-phase cell fraction measurements.

## PATIENTS AND METHODS

### Patients

Patients with untreated NSCLC underwent this study. All 24 patients were treated by tumor resection within 2 wk after the PET study. Twenty of the patients were male and four were female. The mean age was 62.3 yr (range, 46–82 yr). All patients had a tumor >2 cm diameter on CT film. Morphologic classification of the bronchogenic carcinomas was done according to WHO criteria (1981) (22). The tumors were comprised of 12 squamous-cell carcinomas, 10 adenocarcinomas, and 2 adenosquamous carcinomas. The age and sex of the patients, as well as the histological characteristics of the tumor, pathological TNM classification and staging of each patient are summarized in Table 1. Staging was determined by the guidelines of the International Staging System for Lung Cancer (UICC 1987) (23). Informed consent was obtained from patients prior to each PET study.

### Imaging with Carbon-11-Methionine

A whole-body PET scanner, Headtome IV (Shimadzu, Kyoto) (24), was used to image $^{11}$C-methionine uptake. For emission scanning, we customarily employ a 6-mm spatial resolution in a patient cross-section by adjusting the Butterworth filter level. (During transmission, the spatial resolution was adjusted to 12 mm.) The field of view was 512 mm in diameter. The slice thick-

ness of direct and cross planes was 11 mm. The make-up of our machine supplies five slices simultaneously with a slice interval of 13 mm (with a total of 63 mm). During image reconstruction, the image matrix was constructed from data in the central part of the field of view (256 × 256 pixels of 1 mm square on the real scale). The total number of counts for the transmission scan was more than $6 × 10^6$, and at least $1.5 × 10^6$ for the emission scan, for a single field of view.

Emission data were acquired using a respiration-synchronized gating device we fabricated which is connectable to the input trigger system of the PET system. It minimized the partial volume effect caused by respiratory movements; it was monitored by a body impedance pletysmograph ("Respi-trace", Ambulatory Monitoring, NY) while sensing changes in the patient's abdominal circumference. Radioactivity data were accumulated only during the expiratory state for the first third of the respiratory cycle. The transmission scan was performed without respiration gating while the patient was asked to breathe shallowly during scanning. Correct positioning of the patient, placed in the supine position on the PET couch, was achieved with reference to chest x-ray and CT films, and by observation of the transmission image.

Carbon-11-L-methionine was synthesized by Comar's method (25) with a slight modification using L-homocysteine thiolactone instead of L-homocysteine and $^{11}$C-methyliodide during transmission scanning. Carbon-11-methionine (about 10 mCi (370 MBq)) was then injected by bolus into the antecubital vein and flushed with saline. Data were collected at 0–2 min and 10–20 min, separately, with respiration gating and were decay-corrected to time zero automatically. The first time-frame image showed the blood-pool image that facilitated recognition of the anatomical location of blood vessels in the mediastinum. The second time-frame image (later image) showed the area of $^{11}$C-methionine accumulation in the tissue. The $^{11}$C activity trapped in tumors during the first 10 min remained almost constant for 1 hr with decay correction.

The appropriate time period for tumor imaging as described above was determined in a preliminary experiment by measuring the time course of radioactivity of lung tumors (an adenocarcinoma located in the pulmonary apex and a squamous cell carcinoma located in the hilus of the lung), without employing the respiratory gating. We selected these tumors expecting that the influence of respiratory motion to the location of the tumor might be minimal. The radioactivity in the tumor remained unchanged between 10 min and 60 min after bolus injection of $^{11}$C-methionine (Fig. 1).

The cumulative tumor radioactivity was calculated in the region of interest (ROI) placed over the later image. The $^{11}$C uptake was quantitated as follows. First, we displayed the later image on a CRT screen to see the contour of tumor; the color display enabled the radioactivity concentration to appear in different colors. Next, we placed a ROI, corresponding to 1.2 cm$^2$ in body size, over the most radioactive area—usually the center—and obtained the radioactivity concentration in terms of cps/cm$^3$. Carbon-11 uptake was expressed by the differential uptake ratio (DUR) (19) as follows:

$$DUR = \frac{\text{Tissue radioactivity concentration}}{\text{Total injected dose/Body weight}}.$$

The total injected dose was determined from the well-counter count of the injected solution after appropriate dilution, corrected by the cross-calibration factor between the well counter and PET.
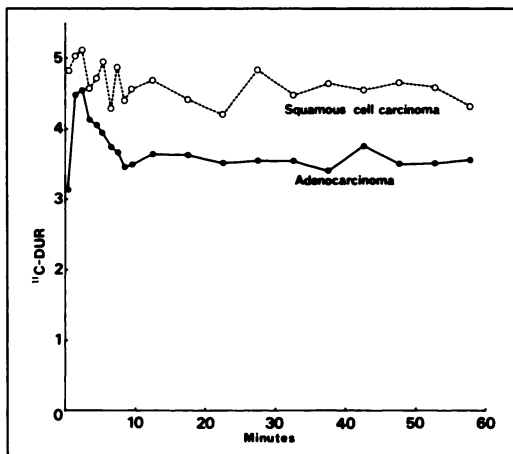
**FIGURE 1.** Typical time course of ¹¹C-methionine uptake in lung tumors. Carbon-11-DUR is the tumor uptake of ¹¹C expressed by the ratio of the tumor concentration of ¹¹C to the hypothetical tissue concentration of ¹¹C where the injected ¹¹C is supposed to be distributed uniformly throughout the whole body. ● = adenocarcinoma; ○ = squamous-cell carcinoma.

## DNA Flow Cytometry

The tumor samples for flow cytometry were taken from the resected lung in order to pick out the tumor tissue from the same position as used for the DUR measurement. Fourteen of the 24 samples were taken from the paraffin-embedded blocks and 10 were taken from the freshly frozen specimens. The samples were examined histologically and determined to be free from contamination with normal pulmonary parenchymal cells.

The following procedure was conducted in collaboration with Otsuka Assay Laboratory, Tokuyama City. When paraffin-embedded blocks were used, four or five 40-μm thick slices were treated by the method of Schutte et al. (21). Normal pulmonary parenchymal cells were used as an internal standard. For the freshly frozen specimen, a 200-mg piece of tumor tissue stored in a deep freezer was cut into small pieces and placed in phosphate-buffered saline. Human normal monocytes were used as a standard. The samples were stained with propidium iodide.

The nuclear DNA content and its histogram were analyzed with a FACSCAN/Cellfit DNA system (Becton-Dickinson, CA). The tumor cell preparation exhibiting only a single G0/G1-peak was regarded as diploid. The DNA index was defined as the ratio of aneuploid G0/G1-peak channel number-to-diploid G0/G1-peak channel number. Histogram samples with a variation coefficient <8% were considered good quality and were subjected to analysis. The count of S-phase and G2/M-phase cells were calculated by the sum of the broadened rectangles (SOBR) method (26) of the Cellfit DNA system.

All the specimens were used for ploidy analysis. Only the freshly frozen specimens were used for analysis of S-phase and G2/M-phase cell population, because the paraffin-embedded blocks are not suitable (21).

## Statistical Analysis

Mean and standard deviation were calculated for each group. The difference of group means was examined with a t-test. Scattered plot was analyzed by linear regression analysis. The coefficient of correlation was analyzed by t-test.

## RESULTS

Table 2 is the list of ¹¹C-methionine uptake (¹¹C-DUR), DNA ploidy, DNA index and the percentage of cells in the S-phase and G2/M-phase of the cell cycle. The ¹¹C-DUR in tumor was always high and demarcated sharply from the surrounding tissue, as seen by direct observation of the resected lung. Figure 2 shows a typical PET image.

There was a significant difference of ¹¹C-DUR between Stage I (mean ± s.d., 3.88 ± 0.47) and Stage II (5.28 ± 0.12, p = 0.001) and between Stage I and Stage IIIA (4.91 ± 1.14, p = 0.025). The ¹¹C-DUR for Stage IIIB (n = 2) was 3.75 and 3.98, and 4.43 for Stage IV (n = 1) (Fig. 3). The cell type difference of NSCLC, however, did not bring about any significant difference in the ¹¹C-DUR value.

Of 24 cases examined, DNA diploidy was found in four while the rest showed aneuploidy with the DNA index ranging from 1.29 to 2.36. There was no multiploidy. Carbon-11-DUR ranged from 3.33 to 3.85 (3.62 ± 0.22) in diploidy cases, and 3.46 to 8.05 (4.78 ± 1.00) in aneuploidy cases. The difference between the two groups was significant (p = 0.0072). The correlation between ¹¹C-uptake rate, ¹¹C-DUR and cellular DNA content at the resting state of cell division was also significant (r = 0.67, p = 0.0003, n = 24) (Fig. 4).

The composition of cells in different stages of the cell cycle was measured in 10 cases, using the freshly frozen specimens. The relationship between the cell-cycle phases and ¹¹C-DUR is as follows: The percentage of S-phase cells correlated with ¹¹C-DUR (r = 0.76, p = 0.010, n = 10) (Fig. 5). A marked correlation was noted between the percentage of proliferative cells (S + G2/M-phase cells) and ¹¹C-DUR (r = 0.86, p = 0.0013, n = 10) (Fig. 6). On the contrary, as a logical consequence, correlation between the sum of percentage of resting cells (G0) plus protein-but-not-DNA-synthesizing cells (G1) with ¹¹C-DUR was inverse (r = −0.86).

Although the purpose of this study was to analyze the relationship of ¹¹C uptake rate in tumors to the proliferative activity of the tumors, we simultaneously examined the effectiveness of the ¹¹C-methionine method as a means of detecting tumor metastasis to the hilar lymph nodes. Carbon-11-methionine PET gave positive images (with DUR >3) in 12 lymph nodes (three patients), which appeared normal in size on CT film but were proven to be a tumor metastasis pathologically (PET true-positive). On the other hand, ¹¹C-methionine PET was false-positive in only two lymph nodes (one patient) of 109 CT-enlarged lymph nodes (27 patients). Following is the description of the only patient with false-positive lymph nodes by PET. This patient (Table 1, Patient 2) had moderately differentiated squamous-cell carcinoma in the right lower lobe. The CT film showed enlargement of pretracheal and subcarinal lymph nodes. With ¹¹C-methionine, the DUR for the tumor was 3.33, and the DUR for the lymph nodes was 3.59 and 3.92, respectively (Fig. 7). Sternum and vertebra bone marrow also exhibited an extraordinarily high uptake in this case.

TABLE 2

**Carbon-11 Uptake After Injection of Carbon-11-Methionine, DNA Ploidy, DNA Index and Cell Cycle Distribution**

| Patient no. | $^{11}$C DUR | Flow-cytometric parameter | | | | Specimen* |
| | | Ploidy | DI | S-phase cells (%) | S + G2/M-phase cells (%) | |
|---|---|---|---|---|---|---|
| 1 | 3.60 | D | 0.98 | — | — | p |
| 2 | 3.33 | D | 1.00 | — | — | p |
| 3 | 3.71 | D | 1.00 | 16 | 17 | f |
| 4 | 3.85 | D | 1.00 | 14 | 20 | f |
| 5 | 3.46 | A | 1.29 | — | — | p |
| 6 | 4.43 | A | 1.33 | 17 | 27 | f |
| 7 | 3.98 | A | 1.36 | — | — | p |
| 8 | 5.35 | A | 1.42 | 31 | 55 | f |
| 9 | 4.23 | A | 1.46 | — | — | p |
| 10 | 3.75 | A | 1.50 | — | — | p |
| 11 | 4.71 | A | 1.52 | 31 | 36 | f |
| 12 | 4.10 | A | 1.63 | — | — | p |
| 13 | 3.46 | A | 1.66 | — | — | p |
| 14 | 4.46 | A | 1.70 | — | — | p |
| 15 | 5.38 | A | 1.78 | — | — | p |
| 16 | 8.05 | A | 1.79 | 87 | 91 | f |
| 17 | 5.16 | A | 1.80 | — | — | p |
| 18 | 5.29 | A | 1.85 | 16 | 25 | f |
| 19 | 5.31 | A | 1.86 | — | — | p |
| 20 | 4.31 | A | 1.90 | 12 | 21 | f |
| 21 | 4.65 | A | 1.91 | 22 | 27 | f |
| 22 | 5.38 | A | 1.93 | — | — | p |
| 23 | 5.05 | A | 1.97 | — | — | p |
| 24 | 5.12 | A | 2.36 | 28 | 35 | f |

*Specimens used for flow cytometry: p = paraffin-embedded (n = 14) and f = freshly frozen (n = 10).
$^{11}$C DUR = $^{11}$C differential uptake ratio, DI = DNA index, D = diploid, and A = aneuploid.

The resected lymph nodes were examined histologically. They were somehow different in appearance from the commonly seen lymph node hyperplasia induced by tumor reaction in that they were occupied by copious lymphoid follicles containing large germinal centers with prominent mitotic activity. Histiocyte clusters were found sporadically between the follicles. Tumor metastasis was not evident in the lymph nodes.

## DISCUSSION

In this study, DNA ploidy and the percentage of proliferative cells of NSCLC were compared with $^{11}$C-methionine uptake rate. We used only freshly frozen specimens (10 samples for the cell-cycle analysis), because paraffin-embedded blocks would contaminate background debris

and cell aggregates (21). The mean percentage of S-phase cells in our specimens (27.4%) was higher than those of other reports (27–30). The highest percentage of S-phase cells (87%) observed in Patient 16 corresponded with the highest accumulation of $^{11}$C.

In order to keep anatomical correspondence between flow cytometry and PET, we worked carefully in cutting out the tumor tissue from the most radioactive area in the $^{11}$C-methionine PET image and rendered it to flow cytometry. This was facilitated by the respiration-synchronized scanning method, which the apparently stopped respiration reduced the partial volume effect on the tumor image.
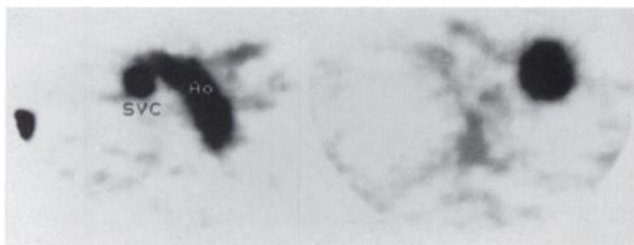


FIGURE 2. (Left) PET vascular image 0–2 min after injection. SVC = superior vena cava and Ao = aortic arch. (Right) PET image of lung tumor (late image) 10–20 min after injection.
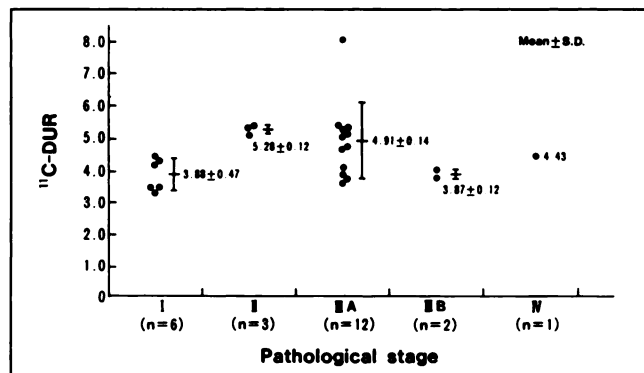


FIGURE 3. Comparison of $^{11}$C-DUR with pathological stages. Each value represents mean and standard deviation.
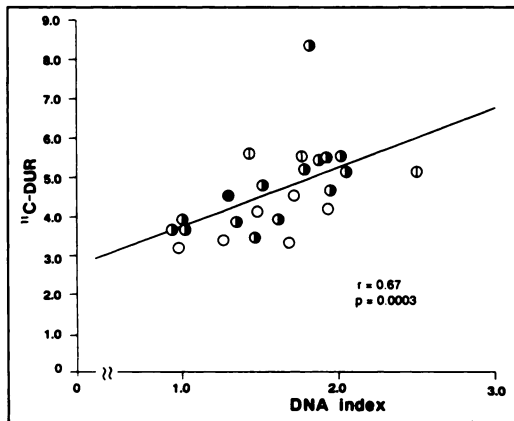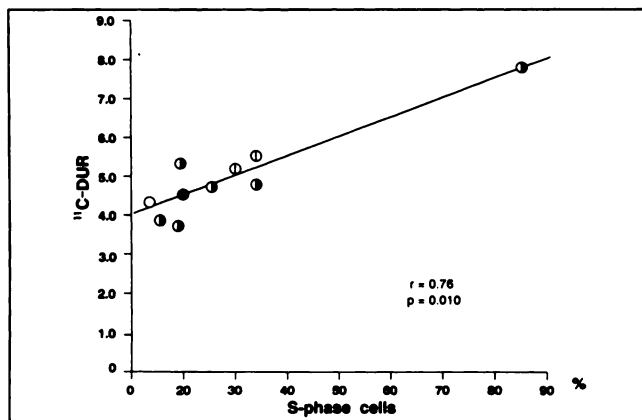
**FIGURE 4.** Correlation between $^{11}$C-DUR and DNA index for 24 NSCLC. O = Stage I; ⊕ = Stage II; ◐ = Stage III; and ● = Stage IV.



**FIGURE 6.** Correlation between $^{11}$C-DUR and proportion of S + G2/M-phase cells (n = 10). O = Stage I; ⊕ = Stage II; ◐ = Stage III; and ● = Stage IV.
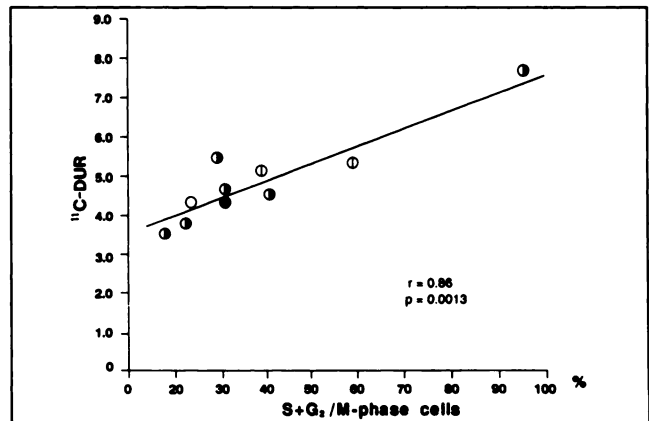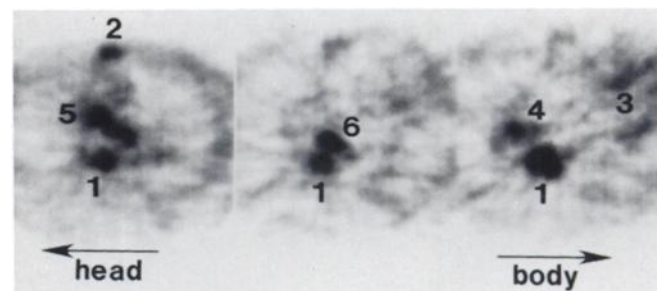
When we used only freshly frozen specimens, a very close correlation between the percentage of proliferative cells and the $^{11}$C-methionine accumulation was observed. If we included (not shown in Results) both freshly frozen specimens and paraffin-embedded specimens (n = 12 instead of 10), the correlation coefficient dropped from 0.76 (p = 0.010) to 0.54 (p = 0.070) for S-phase cells, and from 0.86 (p = 0.0013) to 0.75 (p = 0.0052) for S + G2/M-phase cells.

It is well known that the biosynthesis of methionine is deficient or extremely reduced in malignant tissues (15,16). It follows that the malignant cells have high demands for externally added methionine. Once the $^{11}$C-methionine molecule is taken up in the cell, it will undergo one of the following alternative pathways: integration into protein or incorporation of its methyl group into DNA (addition of methyl group to purine and pyrimidine bases of already formulated DNA molecules) and other compounds.

Proteins within cells are in a continuous steady state of synthesis and degradation (and excretion). Ishiwata et al. (31) reported that, in rats bearing Walker 256 carcinosarcoma, the major tumor cell component for $^{11}$C incorporation after injection of $^{11}$C-methionine was proteins.

Our study in humans demonstrated a close correlation between accumulation of $^{11}$C(methyl)-methionine and incremented cellular DNA content (aneuploidy) in NSCLC. There was also a close correlation between high methionine uptake in tumor and high percentage of proliferative cells in tumor, where the nuclear DNA is duplicating (S-phase), or the DNA content is already doubled (G2/M-phase). This observation seems to suggest a large contribution of transmethylation process to the $^{11}$C uptake in human lung tumors.

It has been verified that nuclear DNA content and the percentage of proliferative cell fraction are corresponding to the aggressiveness of human lung cancer and patient prognosis (2–6). Our study indicated that the measurement of $^{11}$C-methionine uptake would help evaluate the proliferation rate of lung cancer.

The lymphoblasts, either inflammatory or immunoreactive in origin, are methionine-dependent (15,16) and are expected to have a tendency for high methionine uptake. We observed this in one case of mediastinal lymph node enlargement caused by tumor reaction. This lymph node was characterized by a markedly high lymphoblastic proliferation.

Leskinen-Kallio et al. (14) reported that there was no correlation between $^{11}$C-methionine uptake and S-phase



**FIGURE 5.** Correlation between $^{11}$C-DUR and proportion of S-phase cells (n = 10). O = Stage I; ⊕ = Stage II; ◐ = Stage III; and ● = Stage IV.



**FIGURE 7.** A single case of positive uptake of $^{11}$C-methionine exhibited by lymph nodes of nonspecific reactive hyperplasia (histologically proven). 1 = vertebra; 2 = sternum; 3 = myocardium; 4 = lung tumor (DUR, 3.33); 5 = pretracheal lymph node (DUR, 3.59); 6 = subcarinal lymph node (DUR, 3.92).

cell percentage in nonHodgkin's lymphoma. However, a problem seems to be involved with the paraffin-embedded specimens they used for the flow-cytometric analysis, as we previously mentioned. In breast cancer, they also found an association of $^{11}$C-methionine uptake with the size of S-phase fraction (r = 0.77, p = 0.01) (13) using paraffin-embedded specimens. They concluded that the accumulation of $^{11}$C-methionine may correlate with the proliferation rate of breast cancer.

Kubota et al. (32) reported that the radiation response monitored by radiotracer uptake was similar between L-[methyl-$^{14}$C]methionine and [6-$^3$H]thymidine, but very different from the response with $^{18}$F-FDG and $^{67}$Ga in an experiment with a rat tumor model combined with radiotherapy. This observation is suggestive of a close link in the metabolism of methionine and thymidine in the rat tumor.

In summary, NSCLC was visualized with $^{11}$C-methionine. In this tumor type, the intensity of $^{11}$C-methionine uptake was strongly associated with the cellular DNA content and the extent of duplicating DNA (the latter representing the proliferative activity of the tumor). Carbon-11-methionine imaging seems to be a reliable technique for attaining a noninvasive diagnosis of aggressiveness of NSCLC.

## ACKNOWLEDGMENTS

## REFERENCES

1. Akin NB, Kay R. Prognostic significance of modal DNA values and other factors in malignant tumors based on 1465 cases. Br J Cancer 1979;40:210–221.
2. Volm M, Mattern J, Sonka J, et al. DNA distribution in non-small-cell lung carcinomas and its relation to clinical behavior. Cytometry 1985;6:348–356.
3. Volm M, Drings P, Mattern J. Prognostic significance of DNA patterns and resistance-predictive tests in non-small-cell lung carcinoma. Cancer 1985; 56:1396–1403.
4. Zimmerman PV, Tawson GA, Bint NH, Parsons PG. Ploidy as a prognostic determinant in surgically treated lung cancer. Lancet 1987;5:530–533.
5. Tirindelli-Danesi D, Teodori L, Mauro F, et al. Prognostic significance of flow cytometry in lung cancer: a five-year study. Cancer 1987;60:844–851.
6. Volm M, Hahn EW, Mattern J, et al. Five-year follow-up study of independent clinical and flow cytometric prognostic factors for the survival of patients with non-small-cell lung carcinoma. Cancer Res 1988;48:2923–2928.
7. Joensuu H, Klemi PJ, Korkeila E. Prognostic value of DNA ploidy and proliferative activity in Hodgkin's disease. Am J Clin Pathol 1988;90:670–673.
8. Ensley JF, Maciorowski Z, Hassan M, et al. Cellular DNA content parameters in untreated and recurrent squamous-cell cancers of the head and neck. Cytometry 1989;10:334–338.
9. Merkel DE, McGuire WL. Ploidy, proliferative activity and prognosis. DNA flow cytometry of solid tumors. Cancer 1990;65:1194–1205.
10. Minn H, Joensuu H, Ahonen A, Klemi P. Fluorodeoxyglucose imaging: a method to assess the proliferative activity of human cancer in vivo. Comparison with DNA flow cytometry in head and neck tumors. Cancer 1988; 61:1776–1781.
11. Minn H, Paul R, Ahonen A. Evaluation of treatment response to radiotherapy in head and neck cancer with fluorine-18-fluorodeoxyglucose. J Nucl Med 1988;29:1521–1525.
12. Haberkorn U, Strauss LG, Reisser C, et al. Glucose uptake, perfusion and cell proliferation in head and neck tumors: relation of positron emission tomography to flow cytometry. J Nucl Med 1991;32:1548–1555.
13. Leskinen-Kallio S, Nagren K, Lehikoinen P, et al. Uptake of $^{11}$C-methionine in breast cancer studied by PET. An association with the size of S-phase fraction. Br J Cancer 1991;64:1121–1124.
14. Leskinen-Kallio S, Routsalainen U, Nagren K, et al. Uptake of carbon-11-methionine and fluorodeoxyglucose in nonHodgkin's lymphoma: a PET study. J Nucl Med 1991;32:1211–1218.
15. Hoffman RM. Altered methionine metabolism and transmethylation in cancer. Anticancer Res 1985;5:1–30.
16. Judde JG, Frost P. Patterns of methionine auxotrophy in normal and neoplastic cells: the methionine independence of lymphocytic mitogenesis and low frequency of the methionine-dependent phenotype in human tumors. Cancer Res 1988;48:6775–6779.
17. Kano Y, Sakamoto S, Kasahara T, et al. Methionine dependency of cell growth in normal and malignant hematopoietic cells. Cancer Res 1982;42:3090–3092.
18. Bustany P, Chatel M, Derlon JM, et al. Brain tumor protein synthesis and histological grade: a study by positron emission tomography (PET) with $^{11}$C-L-methionine. J Neurol Oncol 1986;3:397–404.
19. Fujiwara T, Matsuzawa T, Kubota K, et al. Relationship between histologic type of primary lung cancer and carbon-11-L-methionine uptake with positron emission tomography. J Nucl Med 1989;30:33–37.
20. Headley DW, Friedlander ML, Taylor IW, et al. Method for analysis of cellular DNA content of paraffin-embedded pathological material using flow cytometry. J Histochem Cytochem 1983;43:3982–3997.
21. Schutte B, Reynders MJ, Blijhan GH, et al. Flow cytometric determination of DNA ploidy level in nuclei isolated from paraffin-embedded tissue. Cytometry 1985;6:26–30.
22. World Health Organization. Histological typing of lung tumors, second edition. Geneva: WHO; 1987.
23. Harmank P, Sobin LH. TNM classification of malignant tumors. Geneva: Union internationale contre le Cancer; 1987.
24. Iida H, Miura S, Kanno I, et al. Design and evaluation of Headtome IV, a whole-body positron emission tomograph. IEEE Trans Nucl Sci 1989;36:1006–1010.
25. Comar D, Carton JC, Maziere M, Marazano C. Labeling and metabolism of methionine-methyl-$^{11}$C. Eur J Nucl Med 1976;1:11–14.
26. Dean PN. Data analysis in cell kinetics research. In: Gray JW, Darzynkiewicz Z, eds. Techniques in cell cycle analysis. Clifton, NJ: Humana Press; 1987:207–253.
27. Raber MN, Barlogie B, Farquhar D. Determination of ploidy abnormality and cell cycle distribution in human lung cancer using DNA flow cytometry. Proc Am Assoc Cancer Res 1980;21:159.
28. Bunn P, Schlam M, Gazdar A. Comparison of cytology and DNA content analysis by flow cytometry in specimens from lung cancer patients. Proc Am Assoc Cancer Res 1980;21:160.
29. Olzewski W, Darzynkiewicz Z, Claps ML, Melamed MR. Flow cytometry of lung carcinoma: a comparison of DNA stemline and cell cycle distribution with histology. Anal Quant Cytol 1982;4:90–94.
30. Teodori L, Tirindelli-Danesi D, Mauro F, et al. Non-small-cell lung carcinoma: tumor characterization on the basis of flow cytometrically determined cellular heterogeneity. Cytometry 1983;4:174–183.
31. Ishiwata K, Vaalburg W, Elsinga PH, et al. Comparison of L-[1-$^{11}$C] methionine and L-[methyl-$^{11}$C]methionine for measuring in vivo protein synthesis rates with PET. J Nucl Med 1988;29:1419–1427.
32. Kubota K, Ishiwata K, Kubota R, et al. Tracer feasibility for monitoring tumor radiotherapy: a quadruple tracer study with fluorine-18-fluorodeoxyglucose or fluorodeoxyuridine, L-[methyl-$^{14}$C]methionine, [6-$^3$H]thymidine, and gallium-67. J Nucl Med 1991;32:2118–2123.